DEM Modeling and Geotechnical Applications

Bruno Chareyre
Laboratoire Sols, Solides, Structures, INPG, UJF, CNRS, Grenoble, France

ABSTRACT

The discrete element method, which represent he soil as a collection of particles, is used intensively for researches on the micro-mechanics of soils, but it is rarely used for modelling soil structures of large dimensions. One reason is that modelling the actual micro-structure of the soil in large scale problems needs to modelise a number of grains that is far too high compared to the memory of current computers. This paper show that the DEM can be used in practical applications however, by upscaling the size of particles. The method to simulate the behaviour of real soils is discussed, and an example application of this concept to soil-geosynthetic structures is detailed. Pull-out tests on anchorages of complex geometries are simulated and the results are compared with experiments. This comparison show that the model is robust and bring out the most important mechanisms of deformation of the structures. Moreover, the model can predict the behaviour quantitatively, e.g. to estimate the ultimate loads on structures.

1 INTRODUCTION

The discrete element method (DEM), as proposed in Cundall and Strack (1979), is a discrete mechanical model in which granular materials are represented as a collection of rigid bodies interacting via contact laws. The DEM has been widely used in the past decades for studying the micromechanics of granular materials, but only few applications of the DEM in full-scale geotechnical problems can be found in the literature. The present paper discusses how the DEM can apply for simulating soil structures, and what are the benefits of such approach.

The DEM is based on micromechanical parameters like the shape of grains or the contact friction, when soil mechanics and measurements mostly describe the behaviour of an equivalent continuum. Consequently, modelling a geotechnical problem with the DEM implies a choice between : 1) defining the model based on real micromechanical parameters, and trying to measure them (incuding aspects such as particle size distribution, shape of grains, or even structural anisotropy at the micro-level); or 2) trying to generate a DEM material which will have the same macroscopic properties than a real soil.

Considering the fact that the current capabilities of computers correspond to simulations with a number of grains between 10,000 and 100,000 in most cases, the first strategy will practically restrict the DEM to problems of very small size or with very large grains (like rockfill dams in Tran et al. (2005)).

The second strategy, on the other hand, can apply in a lot more cases, since it can include an up-scaling of grain sizes, as long as the macroscopic properties of both real and simulated soils remain the same. The paper will discuss, in section 2, how this strategy can be implemented in geotechnical problems; and an example application is proposed in section 3.

2 MECHANICAL PROPERTIES OF A SIMULATED GRANULAR MATERIAL

2.1 *Objectives and methods*

A packing of grains modelised with the DEM can be viewed as a virtual material. In the context of geotechnical applications, the objective is to define a virtual material that will have the same properties than a real soil. It is believed that focusing on few, well defined, mechanical parameters (i.e. elastic moduli, friction angle, cohesion) is the most practical approach, rather than trying to reproduce all aspects of a real stress-strain curve.

This section details the procedure that can be used to obtain stress-strain curves representing the behavior of the virtual DEM materials, to define mechanical parameters, to calibrate the model, and to establish micro-macro relations. Some important as-

sumptions (representativeness and quasi-staticity) will be discussed. In the last part, the relations between the parameters of the model and the parameters of the macroscopic behaviour will be summarized.

2.2 *Modeling a triaxial test*

This section briefly describe the model and the method for modeling a triaxial test on a DEM material. The same method was used for 2D and 3D computations. The grains were modelised as spheres (discs in 2D) or as groups of spheres to obtain more complex geometries, as in fig. 1.

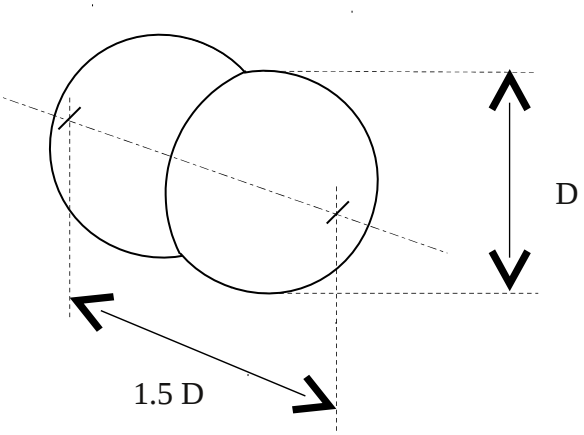

Fig. 1. A typical cluster of spheres for modelling non-spherical grains.

2.2.1 *Contact model*

The contact model consists of a linear stiffness model and a Coulomb–like slip model (Fig. 2). The stiffness model is defined by two parameters: normal stiffness k_n and tangential stiffness k_t. The normal and the tangential components of the contact force are proportional, respectively, to the overlap between two discs in contact and to the tangential displacement at contact. The tangential component of the contact force is limited in magnitude with respect to the Coulomb-like slip model, with friction angle μ. The contact model can include a form of cohesion, with tensile and shear strength at contact.

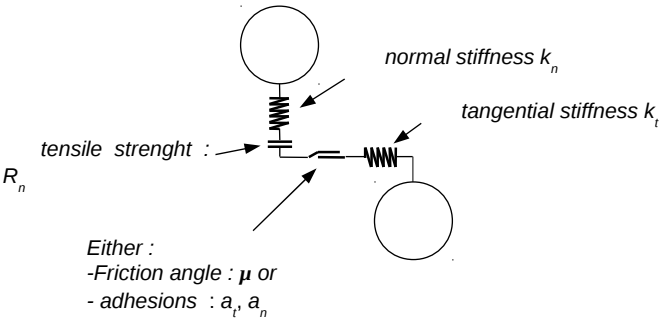

Fig. 2. Contact model.

2.2.2 *Triaxial testing*

Several important stages are required to simulate a triaxial compression test: generating the sample, achieving the desired porosity and then the compression itself.

Generation of the Sample: the positions of the particles were chosen randomly within the volume bounded by four rigid walls defining the contours of the test sample (see fig. 3).

Controlling compacity : after the particle positioning stage, the density of the sample is low (no inter-granular contact). There are then two stages in order to achieve a precise porosity: a gradual increase of the size of the grains, then a compaction of the sample by reducing inter-granular friction until the desired porosity is reached (during this phase, a constant isotropic stress is maintained by adjusting the size of the particles slightly). Once the assembly is stable with the desired porosity, the friction coefficient is set to the value it will have during the test.

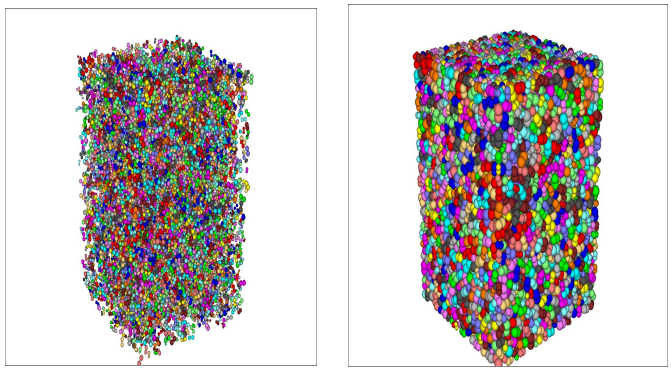

Fig. 3. Random generation of particles (left) and compacted sample (right) for 3D packings.

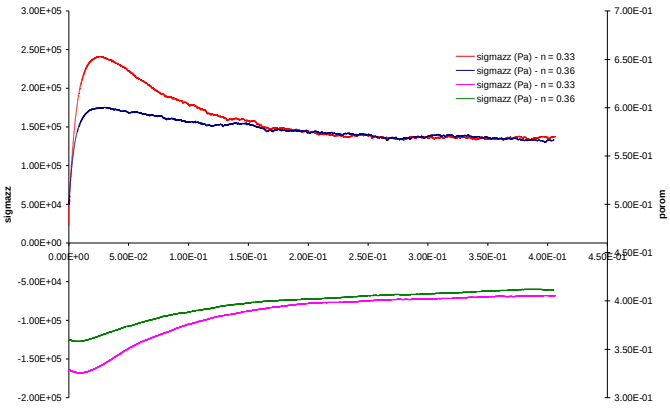

Fig. 4. Evolution of deviatoric stress and porosity in simulated triaxial tests. Two samples with different values of initial porosity are presented.

Triaxial Compression : triaxial compression is simulated by imposing a translation speed on the upper wall while the side walls maintain a constant lateral stress. Grain-wall contacts are non-frictional. The strains and stresses are deduced directly from the displacements and the forces exerted on the walls. Results of triaxial compression tests on a 3D DEM model of spheres are presented on figure 4, for different values of initial compacity.

2.3 *Representativeness*

The first step in the modeling - the generation of the packing - is a random process. Consequently, the σ–ε curve obtained after a simulated test must be considered as an event, in the statistical sense. The representativeness of such curves is discussed here.

The results of two series of computations are reported in fig. 5. One series is performed on samples of 500 grains, the other one is based on samples of 4000 grains. All samples are generated with same parameters, namely the same compacity and the same contact laws. The results with 4000 grains are less scattered than the ones with 500 grains.

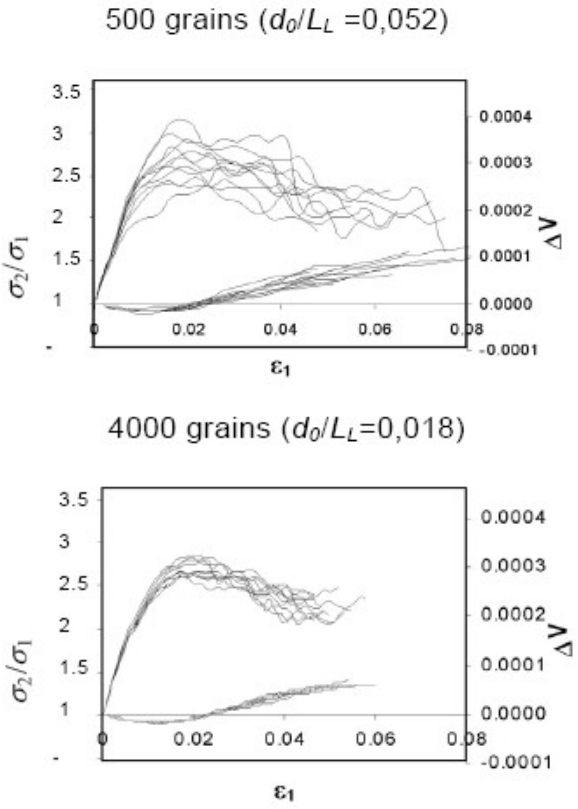

Fig. 5. Dispersion of the results in series of triaxial simulations (2D).

Fig 6. shows that the mean value and the standard deviation of the peak stress in the series of triaxial simulations are linear in term of d_o/L, where d_0 and L are the mean size of the grains and the height of the sample.

The linear evolution of the standard deviation is consistent with the central limit theorem. The linear evolution of the mean peak stress corresponds to a bias in the results, which can be significant with a low number of grains (with 500 grains : 10% deviation compared to σ_∞). This evolution can be explained by boundary effects.

Fig. 6 can be used to determine the minimum number of grains to evaluate σ_p with a sufficient accuracy. Most results presented here are based on more than 8000 grains, which correspond in fig. 6 to a bias of 2.3%.

Note that the result on fig. 6 is only relevant for 2D packings. Similar investigations on 3D sphere packings is still to be done.

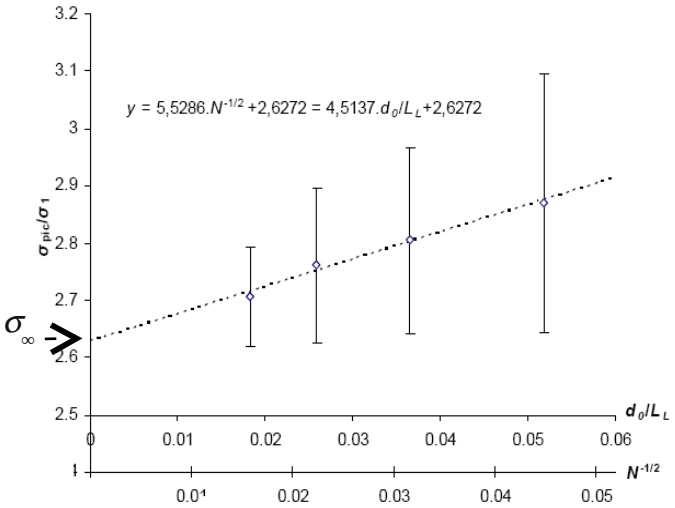

Fig. 6. Statistics of peak stress as function of the size of the sample (2D).

2.4 *Dynamic effects*

The DEM is based on the laws of the dynamics. Consequently, a static equilibrium is always – in a DEM simulation – the result of a dynamic process, in which a form of damping is needed in order to reach a stable solution. The damping can be due to contact friction alone, but a numerical damping is often used for faster convergence. Here the non-viscous damping of Hart et al. (1988) is used. One consequence of the underlying dynamics, is that the results of computations are sensitive to timescale. Fig. 7 shows that stress-strain curve obtained after simulated triaxial tests (2D) is clearly a function of strain rate. This time-dependency can be a problem when one needs to modelize the quasi-static behaviour of a soil or a structure, using the DEM. The question is : “is it possible to obtain a result that is independant on the loading rate?”.

The peak stress values from the curves on fig. 7 are plotted versus strain rate in fig. 8. Other results obtained with different damping are included too. The figure shows a linear relationship between the strain rate and the increase in the apparent peak stress. Morever, for a given strain rate, the stress increase is proportional to the damping coefficient, so that the peak stress can be expressed as :

$$\sigma_{peak} = \sigma_{peak}^{QS} + k.D.\dot{\varepsilon}$$

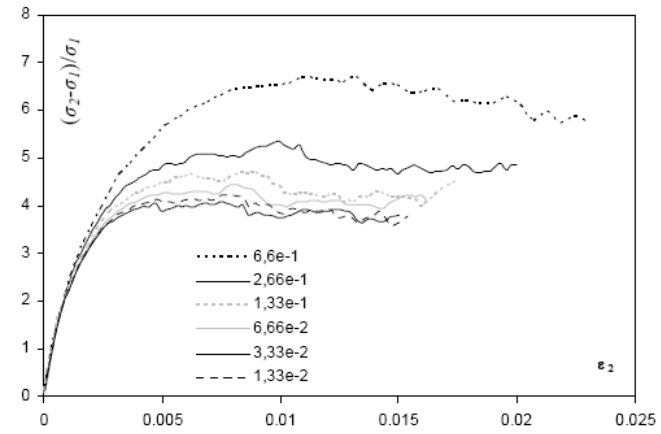

Fig. 7. Influence of the strain rate on stress-strain curves (8000 grains - 2D).

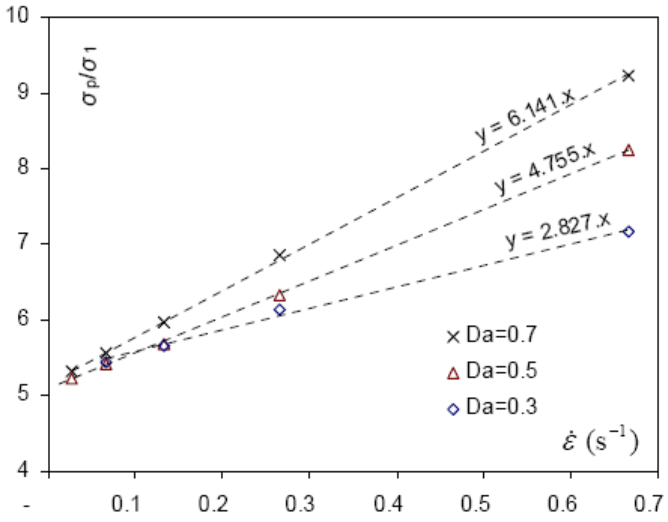

Fig. 8. Influence of the strain rate on the peak stress, as function of the damping coefficient D_a.

Where σ_{peak}^{QS} is the quasi-static limit, and k a constant. Note that k depends on some parameters of the model, namely the density of the grains and the parameters of the contact laws.

One important aspect of eq. (1) is the fact that a bias due to strain rate is inherent in the result, since the strain rate can't be zero. However, the difference between the quasistatic limit σ_{peak}^{QS}, and the apparent peak stress σ_{peak} from the simulation, can be controlled. The simulation can give a good approximation of σ_{peak}^{QS} if the strain rate is small enough.

Note that a strain rate that is considered sufficiently small in the model (here $0.01s^{-1}$ for accurate results) is still very high compared to the strain rate used for triaxial tests on real soils. It denotes the fact that time dependency in real soils is partly due to some aspects that are not modelised in the present DEM model, like viscosity/creep at the scale of contacts.

2.5 *Micro-Macro relations*

The main conclusions of parametric studies that were done on 2D and 3D packings are :

-Micro-macro relations can be expressed independently of the size of particles, thus enabling the use of upscaling techniques.

-Elastic properties of the sample depends on contact stiffness only (k_n and k_t).

-Stress-strain curves are consistent with the critical state theory, with unique values of residual friction and void ratio (see fig. 4).

-Strength parameters can be considered independent on elastic parameters, at least in the range of parameters corresponding to typical soils.

-Peak friction depends on contact friction, density, and the shape of particles.

-Residual friction depends on the shape of particles only.

-Friction angles (peak and residual) in sphere packings is always very low compared to the usual values in soils.

-Complex grain geometries are required to simulate materials with friction angle higher than 22° (see fig. 9). Note that an alternative approach based on enriched contact laws has given good results as well (e.g. rolling friction in Plassiard et al. (2004))

-Adhesion at contact can be used to simulate cohesive and cohesive-frictional soils (fig. 10).

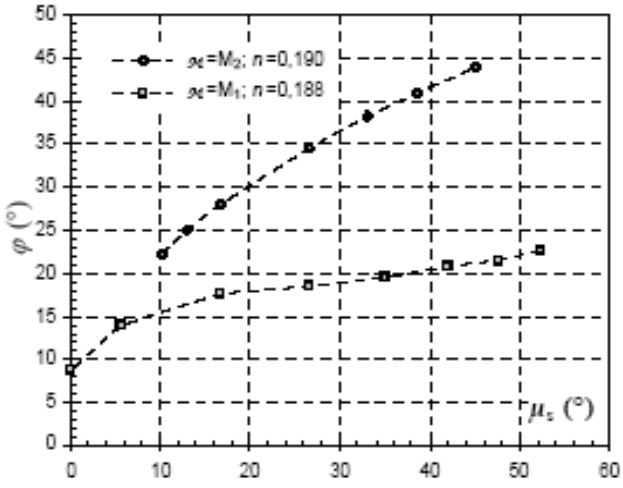

Fig. 9. Relation between contact friction μ and peak friction ϕ in 2D packings, with two different shapes of particules. M1 : grains are modelised as discs, M2 : grains are pairs of discs to simulate elongated particles.

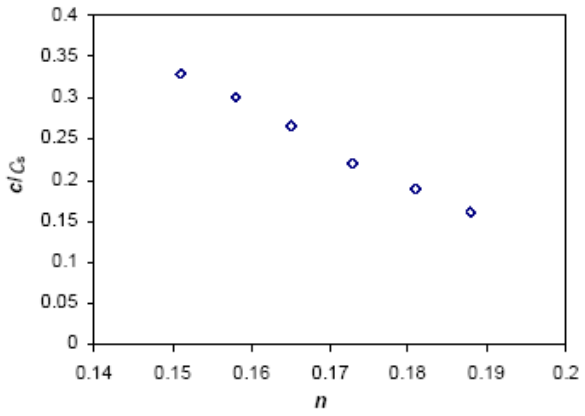

Fig. 10. Coefficient of proportionality between local and global cohesion versus porosity, in 2D packings.

3 EXEMPLE APPLICATION

3.1 *Anchorage of geosynthetics*

Geosynthetics are notably used as liner systems on slopes in a large number of geotechnical applications for reinforcement or watertightness purposes (canal banks, reservoirs, landfills, etc.). The stability of liners depends on the efficiency of the anchorage of the geosynthetics at the top of the slope (fig. 11). The geosynthetic sheets are often installed in trenches to optimise the dimensions of the anchor zone and to ensure effective anchorage. To design the system, it is necessary to estimate the tension that can be mobilised in the anchor (the anchoring capacity) as function of the geometry and the properties of the constituent materials. Due to complex features of failure, this estimation is still problematic.

This being the case, a true scale pull-out apparatus (Fig. 12) was developed at the Cemagref-Bordeaux by Briançon (2000) to investigate the failure behaviour of geosynthetic anchorages. On the numerical side, a model (DSEM) has been developed to modelise geosynthetics. The DSEM and the coupling with the DEM is presented in the first part of this section, then the results of the DEM-DSEM coupling are compared to the experimental results of Briançon.

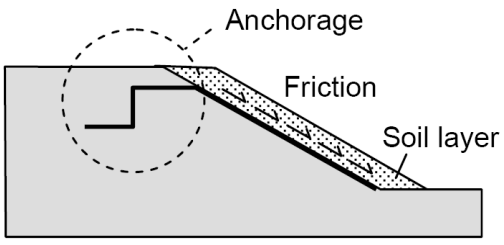

Figure 11. Typical anchorage of a geosynthetic lining system at the top of a slope.

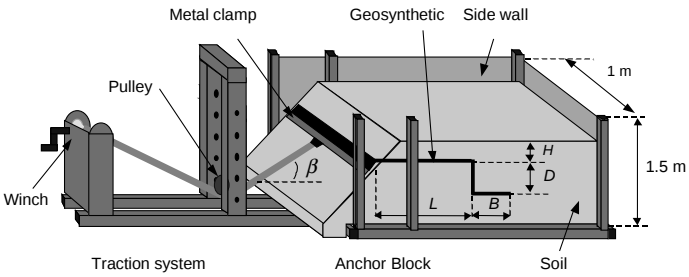

Figure 12. Pull-out apparatus of the Cemagref – Bordeaux (Briançon et al. (2000)).

3.2 *Dynamic Spar Elements*

This section gives a brief overview of the dynamic spar elements (DSEM) that were proposed in Chareyre (2005) to simulate geosynthetic inclusions.

In the DSEM, the motion of each element is determined based on the Newton's second law, using a centered finite difference scheme as in most discrete element methods (see e.g. Cundall and Strack 1979). Consequently, the DSEM may be viewed as an implementation of the DEM, and the formulation detailed in this section is based on concepts that were developed in the DEM related publications of P.A. Cundall. The DSEM's specificities are mainly due to the shape and the deformability of the elements, the type of connection between them, and the inertial model.

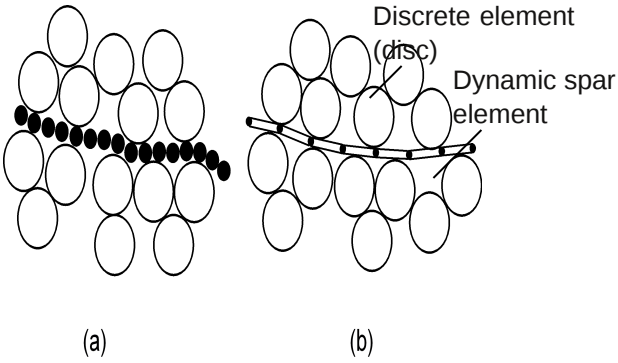

Figure 13. DEM coupled with Dynamic Spar Elements for the modeling of soil-inclusion problems.

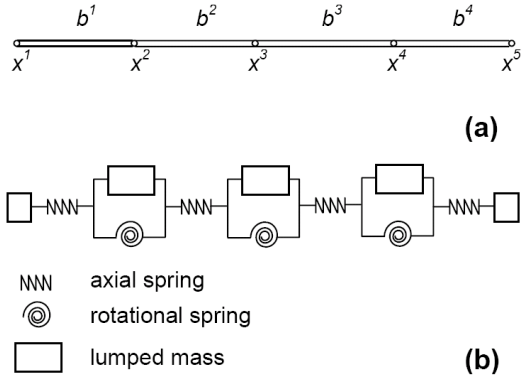

Figure 14. Discretization of an inclusion and inertial model.

3.2.1 *Discretization*

The inclusion is represented by a set of spar elements connected by nodes, as in Fig. 14.a. The length of the elements is considered variable, the axial deformation being accounted for by a variation of the distances between the nodes; the flexion of the inclusion is represented by rotations at the nodes; the flexion of an individual element is not considered. From the inertial viewpoint, the inclusion is treated as a set of lumped masses coinciding with the nodes. This rheological model is illustrated in Fig. 14.b.

3.2.2 *Intrinsic behaviour*

The magnitude of the tensile force in the q-th element is related to the elongation of the element in eq. (1). This definition implies that the inclusion can carry tensile forces only (i.e. positive).

$$T^q = \max\left[J.\varepsilon^q\,;\,0\right] \tag{1}$$

The resultant force vector on an arbitrary node q is the sum of the tensile force vectors T_i^q and T_i^{q+1} in elements q-1 and q. A gravitational forces $m^q g_i$ may also be considered, m^q being the mass of node q. Consequently, the second Newton's law applied to node q writes

$$\ddot{\mathbf{x}}_i^q = \left(T_i^{q-1} + T_i^q\right)/m^q + g_i \tag{2}$$

3.2.3 *Mechanical coupling*

The constitutive behaviour of grain-inclusion contacts is defined by normal and tangential stiffnesses k_n and k_s and the friction angle δ. Thus, contact forces can be computed from the relative displacements at contacts.

The DSEM is coupled with the DEM code by considering the grain-inclusion contact forces f_i^k as external loads on the inclusion. Thus, if n contacts exist on elements q-1 and q, eq. (2) becomes

$$\ddot{\mathbf{x}}_i^q = \left(T_i^{q-1} + T_i^q\right)/m^q + g_i + \sum_{k=1,\ldots,n} \xi^k f_i^k \tag{3}$$

were ξ^k varies lineary between 1 and 0 when the position of contact point k moves from node q to node q+1.

For each contact, a forces $-f_i^k$ is introduced as an external load on the grain corresponding to contact k.

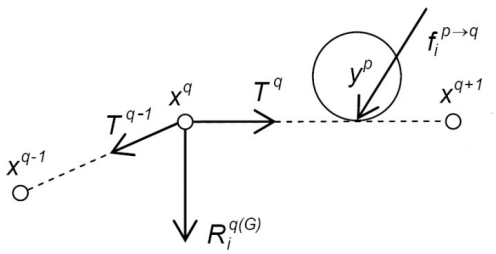

Figure 15. Different types of loads participating to the resultant force on a general node.

3.3 *Numerical versus true-scale experimental modelling*

In this section, predictive computations are presented are contrasted against a series of tests presented in Chareyre et al. (2002).

3.4 *Modelling the actual behaviour of the materials at the macro-scale*

3.4.1 *Soil model*

The particle size distribution (polydisperse) was fixed independently of the actual distribution. Triaxial compression tests were simulated to calibrate micro-macro relations in the particular case of the size distribution choosen. This calibration, together with dimensional analysis, enabled us to choose appropriate micro-parameters so that the triaxial tests simulated fit the behavior of the actual soil at the macro-scale (and at the macro-scale only). In figure 16, the results of triaxial simulations after the contact laws has been set are compared with the experimental failure criterion obtained for the sand.

Note that the soil was modelized with clusters (see Fig. 17) rather than single discs, to reach high values of internal friction angle. Each cluster was made of two discs with a slight difference in sizes (sizes ratio equal to 0.9). Clusters were generated in two different sizes, with a proportion of four small clusters for each large cluster (twice larger).

Table 1. Properties of the soil used in the experiments.

parameter	cohesion	Friction angle	Density
	c (kPa)	ϕ (°)	ρ (kg.m^{-3})
sand	0	41	16.7×10^3
sandy silt*	13	34	18.5×10^3

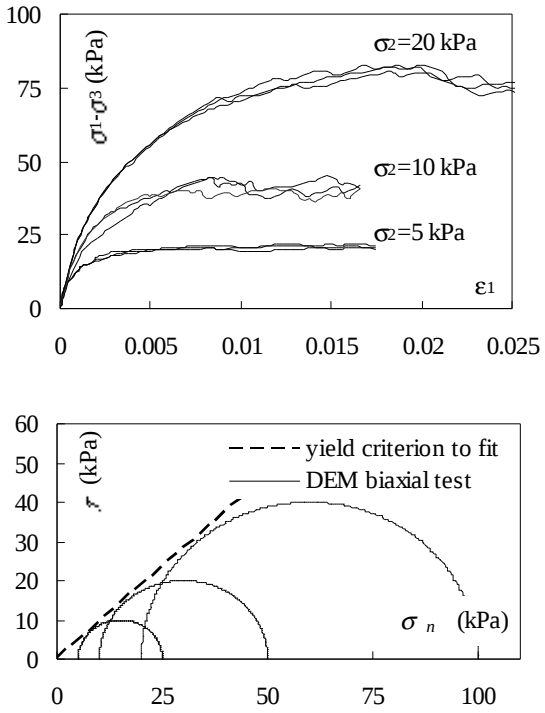

Figure 16. Stress-strain curves obtained after simulating triaxial compressions with the sand model (3 samples with 4000 clusters each) and comparison with experimental yield criterion.

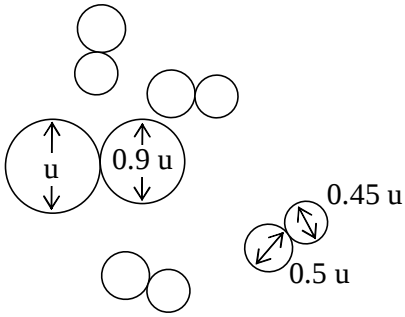

Figure 17. Clusters used to simulate the soil materials

3.4.2 *Soil-inclusion interface*

The macroscopic friction ratio at the soil-inclusion interface was measured in shear tests. It was found equal to 34° (the value was the same for sand-inclusion or silt-inclusion interfaces).

In the DEM-DSEM coupling, the macroscopic interface friction simulated correspond to the local friction δ, so that δ was defined directly from the results of the shear tests : 34°.

The stiffness of the soil-inclusion contacts was taken equal to the stiffness of the soil-soil contacts.

3.5 *Results*

One important result of the tests was that the failure mechanism was strongly influenced by the nature of the soil. A significant deformation was observed with the sand (Fig. 8) while far less deformation was observed in the silt (the failure being essentially due to slippage at the soil-inclusion interface in that case). Fig. 9 shows the geometry of the anchorage simulated, at initial state and after the pull-out simulation, with the parameters corresponding to the silt (soil 1) and the sand (soil 2). The results are in good agreement with the experimental observations : little deformation of the silt, large deformation of the sand.

More important : the evolution of the tensile load T during the pull-out process is correctly predicted by the simulations. Particularly, the maximum value of T, which defines the anchoring capacity, is predicted relatively well with respect to the complexity of the problem.

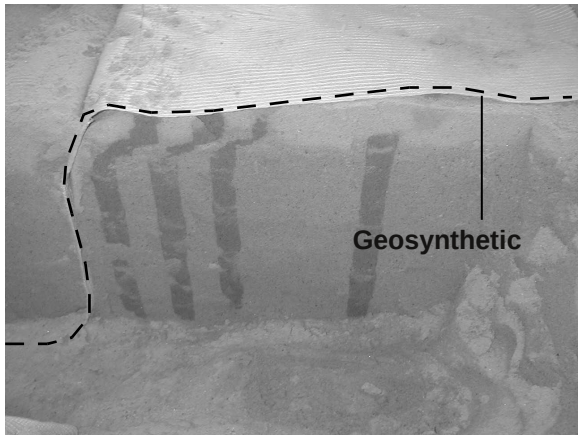

Figure 18. Deformation of the anchoring sand mass after the pull-out test evidenced by colored sand columns (initially vertical).

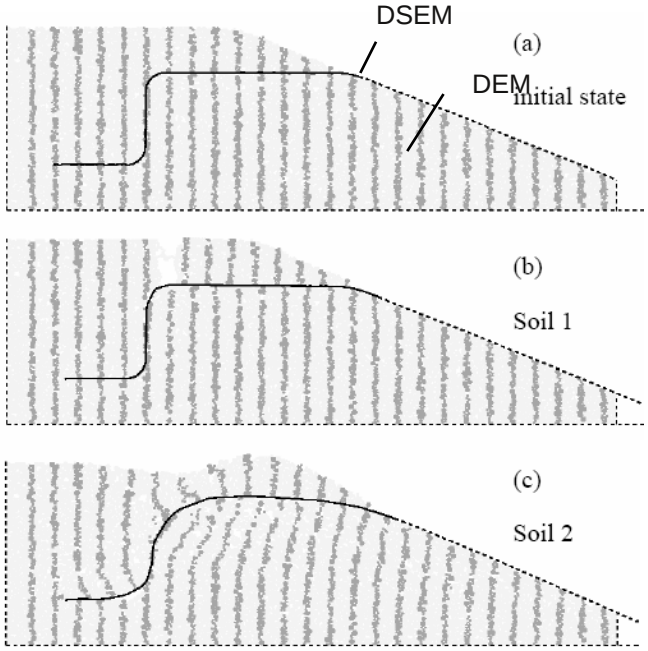

Figure 19. Initial state (a) and simulated evolution of L-shaped anchor with Soil 1 (b - silt) and Soil 2 (c - sand).

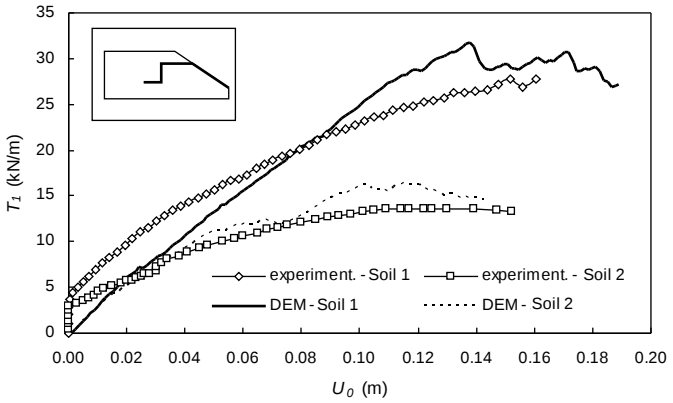

Figure 20. Comparison between the tests and the simulations for L-shaped anchor and both types of soil.

4 CONCLUSION

The behaviour of granular assemblies simulated with the DEM is very similar to the behaviour of soils. However, the classical model in which grains are represented by spheres is not rich enough to simulate materials with high internal friction, like a typical sand. But considering grains with more complex shapes can overcome this difficulty.

Triaxial tests can be simulated DEM materials and can give robust results when the size of the sample and the strain rate are defined adequately. The results of such tests enable the definition of micro-macro relations for calibrating the model. Then, a DEM model can be defined in order to reproduce the macroscopic behaviour of arbitrary frictional and/or cohesive soils, modelling the real microstructure being not a necessary condition.

This approach has been applied for modelling the behaviour of soil-inclusion structures and it has provided good result. Force-displacement curves where predicted correctly, and the failure mechanisms obtained in the simulations where very similar to the ones observed in experiments.

It appears that the DEM is particularly well suited for composites structures, and more generally for problems including strong discontinuities, interfaces, fractures, creation and loss of contacts.

The current capabilities of computers is such that most problems will be better treated with 2D models, as 3D models would require a larger number of elements. In the future however, advances in computer technologies and researches on DEM models (with a richer description of shapes and contact laws) can probably allow more applications in the field of geotechnical engineering.

REFERENCES

Cundall, P.A., Strack O.D.L. (1979). "A discrete numerical model for granular assemblies." *Geotechnique*, 29(1), 47-65.

Tran. T.H., Dedecker. F., and Cambou. B., "Discrete creep model for long-term behaviour of rockfill dams", in *Powders and Grains 2005*, Stuttgart, 2005, Vol.1, pp. 677-680.

Briançon, L., Girard, H., Poulain, D. and Mazeau, N., "Design of anchoring at the top of slopes for geomembrane lining systems", *2nd European geosynthetics conference*, Bologna, Italy, 15-18 october 2000, Vol. 2, pp. 645-650.

Chareyre, B., Briançon, L., and Villard, P., 2002. "Numerical versus experimental modelling of the anchorage capacity of geotextiles in trenches". *Geosynthetics International*, 9(2): 97-123.

Villard, P., Chareyre, B., 2002. "*Discrete element modelling of curved geosynthetic anchorages with known macro-properties"*. Proc. of the First International PFC Symposium, Gelsenkirchen, Germany. 6/7 November 2002. Konietzky (ed): 197-203.

Chareyre, B., Villard, P., 2005. "Dynamic Spar Elements and DEM in 2D for the modelling of soil-inclusion problems". *Journal of Engineering Mechanics - ASCE*. In press.

Hart, R., Cundall, P.A., and Lemos, J. (1988). "Formulation of a three-dimensional distinct element model. II : Mechanical calculations for motion and interaction of a system composed of many polyhedral blocks." *Int. J. Rock Mech., Min. Sci. & Geomech. Abstr*., 25(3), 117-125.

Plassiard J.P, F.V. Donzé & P. Plotto, "High energy impact on embankments - A numerical discrete approach", *Proc. IX Symposium on Numerical Models in Geomechanics*, IX NUMOG Symposium on Numerical Models in Geomechanics Ottawa, 25-27 August 2004.